Oxide Morphology and Spalling Model for NiAl

JAMES L. SMIALEK

The kinetics of Al_2O_3 growth and spalling were observed for Ni-42 at. pct Al oxidized in air at 1100°C up to 1500 h. While crystallographic voids formed at the oxide-metal interface due to the oxidation process, the oxidation resistance was good in 1 h cycle tests. Spalling to bare metal was the predominant mode of oxide loss. The Al_2O_3 grain size at the metal interface varied with a time-exponent of 0.2. In isothermal tests the oxide thickness was nearly parabolic with time, having a time-exponent of 0.40, while the volume per void varied directly with residence time underneath intact oxide. The total void volume accounted for ~1/2 the aluminum needed to form the Al_2O_3 scale. In 1 h cycle tests the oxide thickness and volume per void reached a plateau at ~150 h due to the spalling process. The correlation between total void volume and oxide volume was eventually obliterated by extensive cycling. A cyclic step-process spall model was used to predict the parabolic rate constant, k_p, and the oxide spall fraction, k_s, from gravimetric curves. Predicted values of k_p agreed well with experimental values, while predicted k_s values were often less than measured values. According to this model the severity of a long time test can be rated according to the factor $f_{Me}\sqrt{k_s \cdot k_p \cdot \Delta t}$ mg/cm^2 · cycle, where f_{Me} is the ratio of metal-to-oxygen in the oxide and Δt is the cycle time. Measured values of k_s in isothermal tests varied linearly with exposure time or approximately with (oxide thickness).[2] Cyclic tests showed more scatter and less dependence of k_s on oxide thickness, presumably due to the complex oxide topography and relaxed stress states.

CYCLIC oxidation studies in the MCrAlY systems have shown that the beneficial effects of active metal additions are due to minute effects at the Al_2O_3 oxide-metal interface—including oxide pegging via Y_2O_3 and the prevention of void formation.[1,2] While inferior to some NiCrAlY alloys, NiAl has also proved itself to be a very oxidation resistant material. Studies at the NASA Lewis Research Center have dealt with mapping of cyclic oxidation resistance in the NiCrAl system and have shown that Ni-40 at. pct Al is near the boundary for accelerated oxidation.[3,4] Work here has also been concerned with the case of various oxide spalling models based on a) a continuous loss of oxide,[5] b) a step-process assuming a constant fraction of oxide thickness spalled each cycle,[6] and c) another step-process assuming a constant fraction of oxide area spalled each cycle.[7] The purpose of the present work was to study in detail the Al_2O_3 oxide morphology and oxide-metal interface of a nickel-rich NiAl alloy with the hope of providing information relevant to spalling theories in the MCrAlY system. A second purpose was to study the kinetics of spalling as a critical evaluation of one of the step-process spall models as well as to obtain the experimental data.

MATERIALS AND PROCEDURE

The material used for this program was made from aluminum shot and nickel 270 sheet, both 99.99 pct pure. A 2 × 7 × 7 cm casting was produced by tungsten arc melting in argon. The charge composition was 40 at. pct aluminum; wet chemical analysis of the casting was 41.8 ± 0.2 at. pct (24.8 wt pct). The casting was sectioned and machined into 0.3 × 1.5 × 2 cm test coupons. Surfaces were polished through 3 μ diamond except for long term (500 and 1500 h) cyclic oxidation specimens which were finished with 600 grit emery.

Furnace oxidation tests were run in 1 atm air at 1100° ± 5°C. Cyclic tests involved 1, 20, and 50 h heating cycles, all with 20 min cooling to ~65°C.

Morphologies of resultant oxide and metal surfaces were examined in a scanning electron microscope equipped with an energy dispersive spectrographic (EDS) unit. Accelerating voltage was 25 kV. Cyclic tested specimens were examined after intervals ranging from 1 to 1500 h of exposure, and isothermal specimens were examined from 2 min to 200 h of exposure.

RESULTS AND DISCUSSION

I. SEM Observations

A. Morphology of Oxide and Metal Surfaces. Oxide and metal structures were conclusively differentiated from each other by EDS. Oxide structures exhibited high relative aluminum intensities (Al/(Ni + Al) ≥ 0.5), being for the most part Al_2O_3. Intensities of 1.0 were not observed because *in situ* oxides were not fully opaque to 25 kV electrons, and excitation of nickel in the substrate still occurred. As-polished NiAl or bare metal exposed by oxide spalling typically had relative aluminum intensities of only 0.1 to 0.2. The specimen tilt used in the micrographs was 20 deg unless indicated otherwise. Figure 1 summarizes the sequence of structural changes with increasing oxidation times. At 4.5 min arrays of what appear to be polyhedral voids in the metal were aligned with polishing marks. At this point the oxide was so transparent that it could not be differentiated from the base metal. (No structure was observed at 2 min other than the polishing marks themselves.) After 20 min the specimen was completely covered with a textured oxide which also

JAMES L. SMIALEK is Research Engineer, NASA Lewis Research Center, Cleveland, Ohio 44135.

Manuscript submitted May 27, 1977.

ISSN 0360-2133/78/0310-0309$00.75/0

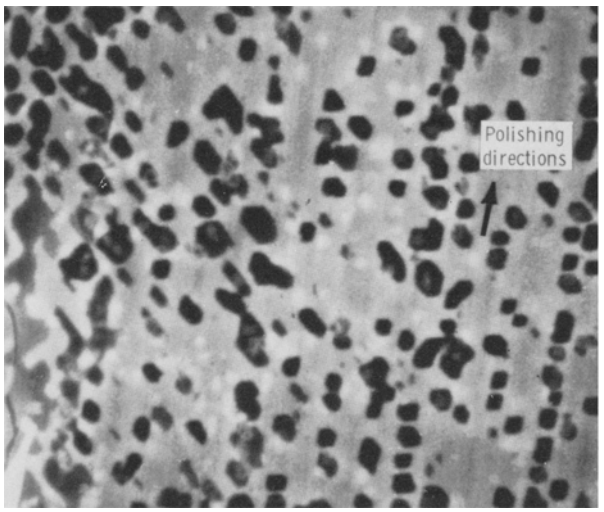

(a)

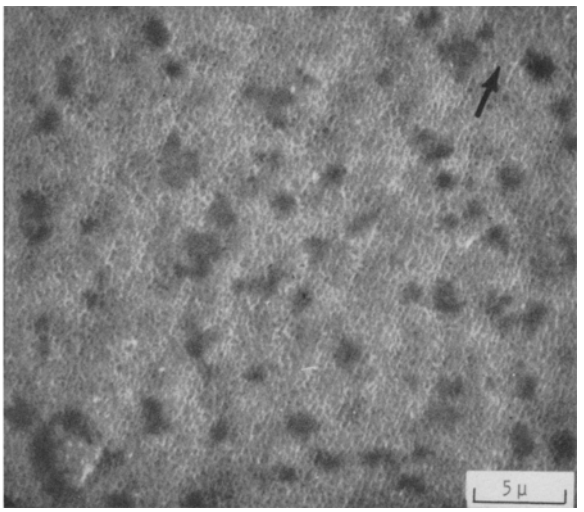

(b)

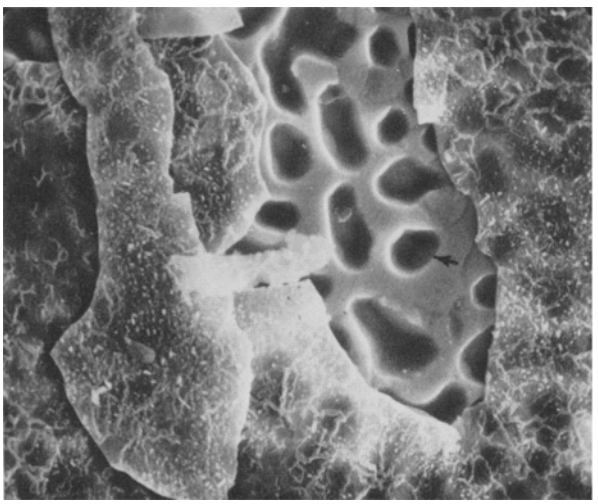

(c)

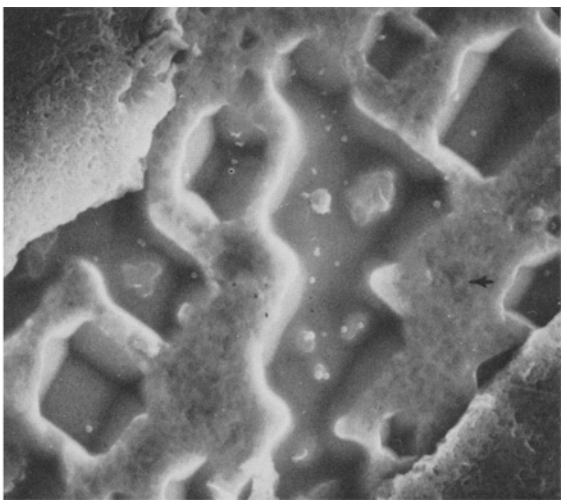

(d)

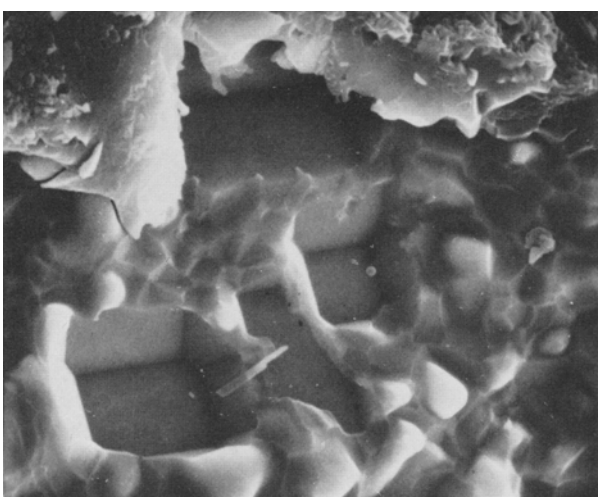

(e)

Fig. 1—Changes in Ni-42Al surface void structures with oxidation time at 1100°C. Magnification 2400 times. (*a*) Initial void arrays, 4.5 min, (*b*) complete oxide covering, 20 min, (*c*) prismatic voids first exposed by spalling, 1 hr, (*d*) formation of oxide imprints between voids, 9 1-n cycles, (*e*) mature metal topography, 1500 1-h cycles.

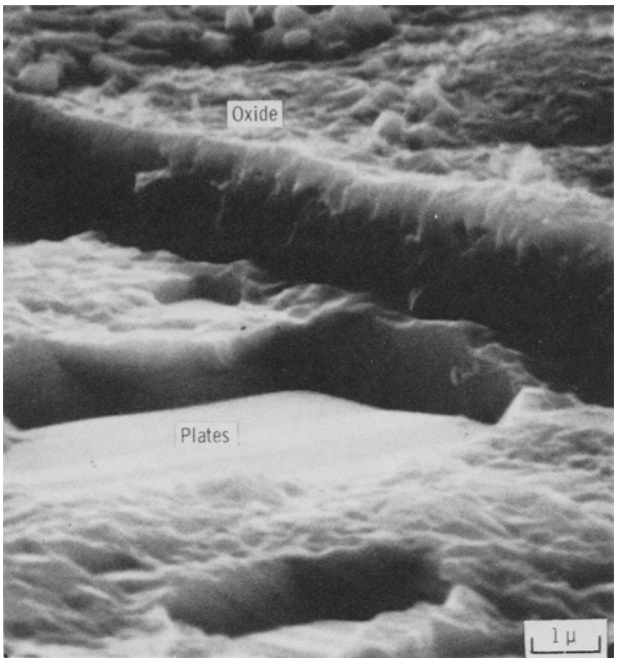

(a)

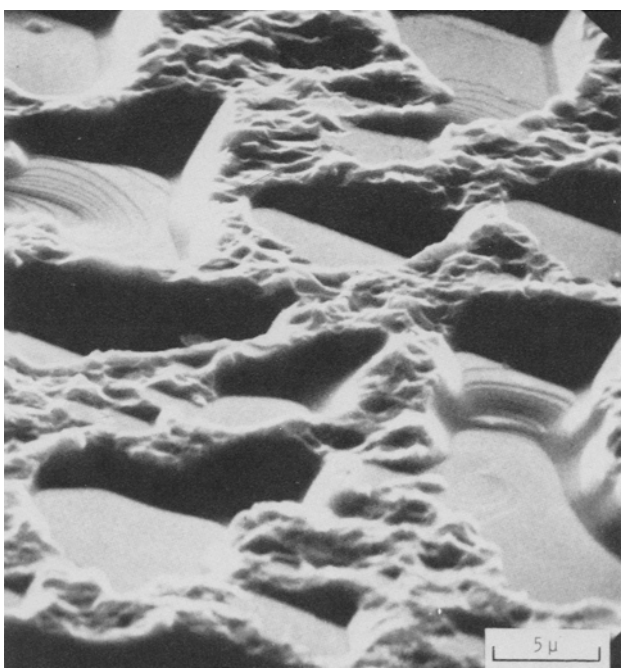

(b)

Fig. 2—Details of void structure in Ni-42Al oxidized at 1100°C, 70 deg tilt. *(a)* Martensite plates, 1500 1-h cycles, magnification 8100 times, *(b)* thermal grooving, 100 h isothermal exposure, magnification 2400 times.

indicated the direction of polishing. The size of this lace texture, 0.4 μ, agrees with the oxide grain size as determined by transmission microscopy of stripped oxide. Larger dark areas indicated where voids probably lay beneath the oxide. After 1 h a spalled oxide flake was apparent, and the exposed metal revealed the beginnings of facets in the voids. Longer test times accentuated the polyhedral nature of the voids (Figs. 1(*d*) and (*e*)) and revealed a definite crystallographic alignment of all the void planes within one grain of the substrate. The faceted nature of the voids probably arises from the preferred growth along the low-energy high-ordered {110} planes in β-NiAl, which intersect at 120 deg angles. While voids were observed in oxidized γ/γ′ NiCrAl alloys,[1,2] they were flatter and less faceted. The regions between the voids exhibited imprints of the oxide in contact with the metal and grew considerably with time, similar to imprints observed in the MCrAl systems.[1,2] As expected, no evidence of oxide pegging was observed in this pure Ni-Al alloy. In numerous high angle photographs of all the specimens, the oxide over the void areas was never observed to be thinner than the oxide in contact with the metal. Also, the voids were not oxidized unless exposed to the atmosphere by oxide cracking or spalling.

Some additional details of the void structure are shown in Fig. 2. Surface shear plates similar to those of martensite were observed after long exposures. Martensitic NiAl has been observed at room temperature for compositions ≤37 at. pct Al.[3] Therefore long-time oxidation may have reduced the surface aluminum content from 42 pct and allowed some martensite to form. The spiral step formations in Fig. 2(*b*) resemble etch pit formations on emergent screw dislocations. The classic etch pit phenomenon involves layer-by-layer material removal from the exposed end of a dislocation. Thus, these step formations suggest that the voids were growing by vapor transport of aluminum from the void surface to the oxide.

Examples of typical oxide structures are shown in Fig. 3. The "lacey" oxidation in Fig. 3(*a*) was observed at areas exposed for short times (*cf*, 1 h oxidation in Fig. 1(*c*)). The fact that these are oxidized voids after 20 test cycles suggests that the original oxide layer had cracked and exposed these voids before spalling off completely on the 20th cycle. A more mature lace structure is shown in Fig. 3(*b*) for 1500 h oxidation. It is apparent that the lace network impinges on itself and forms a more uniform oxide layer. The outer surface of intact thicker oxides often exhibited a porous character that was accentuated by 1200 deg testing as shown in Fig. 3(*c*). The overall structure of void, lacey oxide, and original oxide plates is shown in Fig. 4 for a 20 h exposure. A considerable amount of spalled oxide debris is also apparent. Areas where the lacey oxide has grown over the void structure have resulted in a pocky rough oxide layer. Generalizing, specimens oxidized for a few cycles showed more areas of the original uniform oxide layer, while specimens oxidized for many cycles (~500 h) had very little of the original oxide layer left and were topographically very complex.

Oxide plates were stripped from the substrate using cellophane tape to permit examination of the oxide-metal interface. Typical features of the oxide undersides are shown in Fig. 5. At 1 h (Fig. 5(*a*)) a definitive lace network outlined oxide grain boundaries, implying preferential oxygen diffusion at these areas. A more mature structure developed after 20 h (Fig. 5(*b*)) with porous areas bearing an explicit relationship with the rectilinear arrays of voids seen in the metal. The implication of these porous oxides over the voids is that aluminum transport from the metal to the oxide (presumably vapor transport) was somewhat slower than diffusion at areas of oxide-metal contact. The areas of contact began to exhibit a granular texture

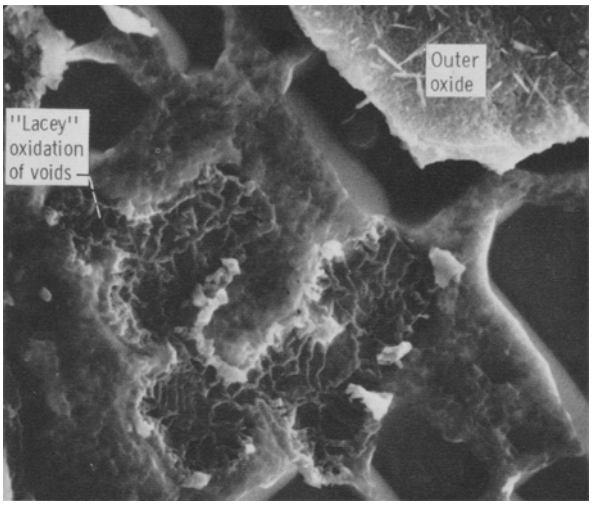

(a)

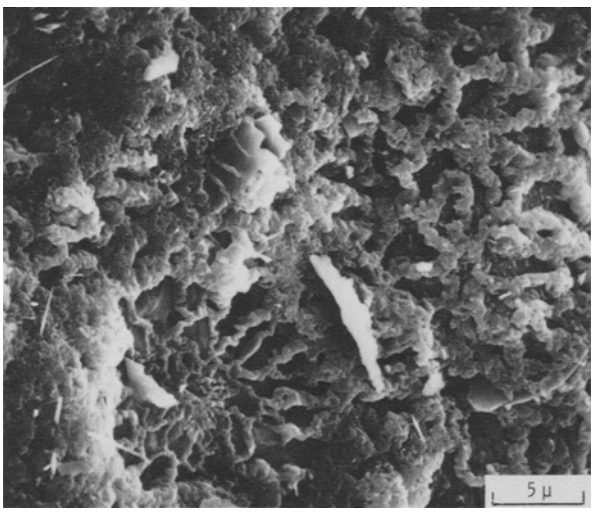

(b)

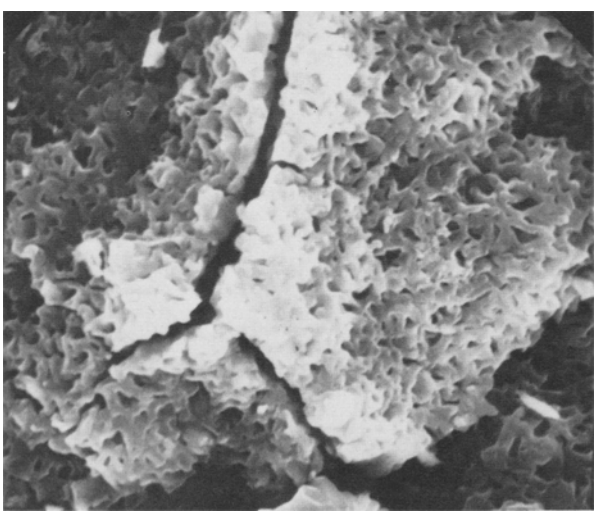

(c)

Fig. 3—Oxide surface structures on Ni-42Al. Magnification 2400 times. (*a*) "Lacey" oxidation of exposed voids, 1100°C/20 h, (*b*) coarse "lacey" oxide, 1100°C/1500 h, (*c*) porous external surface, 1200°C/217 h.

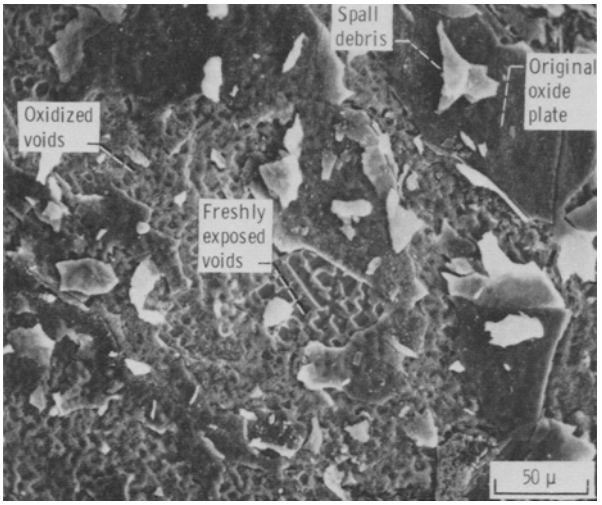

Fig. 4—Typical overall surface structure of Ni-42Al oxidized at 1100°C for 20 1-h cycles.

which was enhanced after 500 h (Fig. 5(*c*)). The fracture edge of this plate was also intergranular in nature. It is apparent that the grain size was an order of magnitude smaller at the gas surface than at the metal surface similar to observations in the NiCrAlY system.[2]

Thin, stripped oxides were also examined by transmission electron microscopy after oxidation times up to 20 min. The grain size as determined by TEM of thin oxides and by SEM of the granular oxide-metal interfaces was observed to increase to ~2 μ as shown in Fig. 6. Theories of grain growth predict parabolic kinetics based on surface energy considerations of the grain boundary: $D = (k_o \exp -Q/RT) \cdot t^n$ (Ref. 9) where D is the average grain diameter, Q is the activation energy for grain boundary diffusion, and $n = 0.5$ for pure materials. (In sintering Al_2O_3 powder compacts, n was found to be only 0.33 due to the restraining effect of pores on boundary motion.[10]) The time-exponents, n, found in Fig. 6 were 1.0 for initial oxidation (TEM) followed by 0.2 for longer test times. No explanation for the relatively low growth rates is apparent from this study. It is interesting to note that the cyclic and isothermal data for Ni-42Al, as well as the limited data for isothermal NiCrAl and NiCrAlY appear to lie within the scatter of the same curve.

Oxide buckling and spalling have been shown to occur due to lateral Al_2O_3 growth and resultant compressive stresses in scales formed on FeCrAl at 1200°C.[11] This lateral growth was associated with an equiaxed oxide grain structure. The cause of lateral growth was said to be the result of nearly equal oxygen grain boundary and aluminum bulk diffusion rates. Oxide growth thus occurred within the body of the scale. On the other hand, the addition of 0.82 wt pct yttrium caused the formation of columnar oxide grains. These grew at the oxide-metal interface, presumably because of a reduction of aluminum diffusion with respect to oxygen diffusion. The mechanism by which yttrium prevented aluminum diffusion in the oxide is not known. Wrinkled, spall-prone equiaxed Al_2O_3 scales were also observed on NiCrAl and CoCrAl, while adherent columnar Al_2O_3 scales formed on NiCrAl and CoCrAl with 0.1 wt pct yttrium additions.[2]

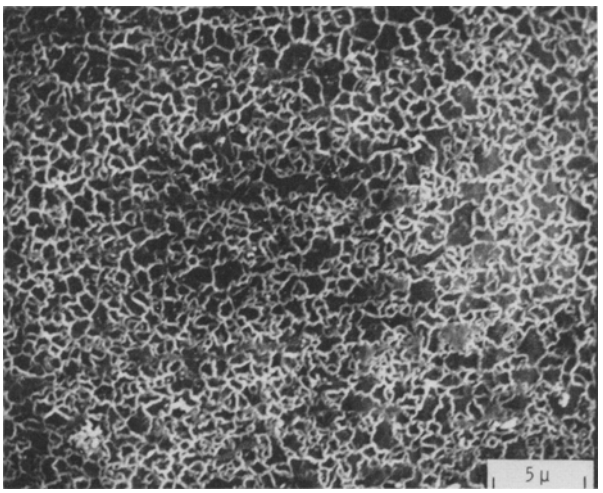

(a)

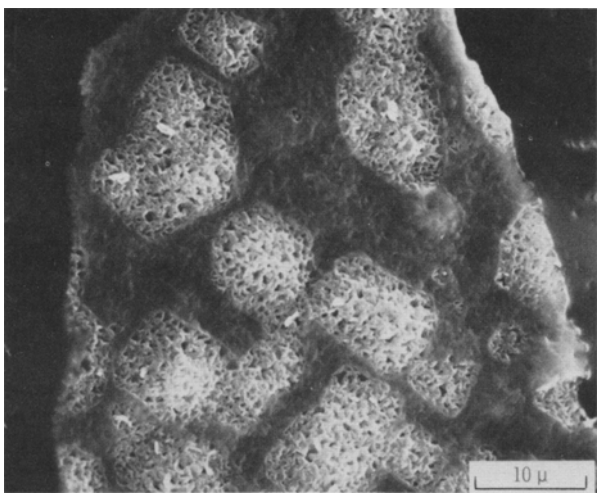

(b)

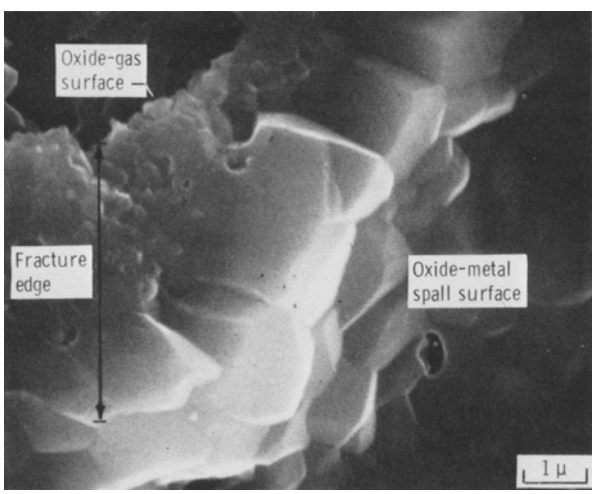

(c)

Fig. 5—Changes in oxide morphology at the oxide-metal interface of Ni-42Al oxidized at 1100°C in 1 h cycles. (*a*) Initial "lacey" network, 1 h; magnification 2400 times, (*b*) porous areas over voids, 20 h; magnification 1500 times, (*c*) grain structure in contact with metal, 500 h; magnification 8100 times.

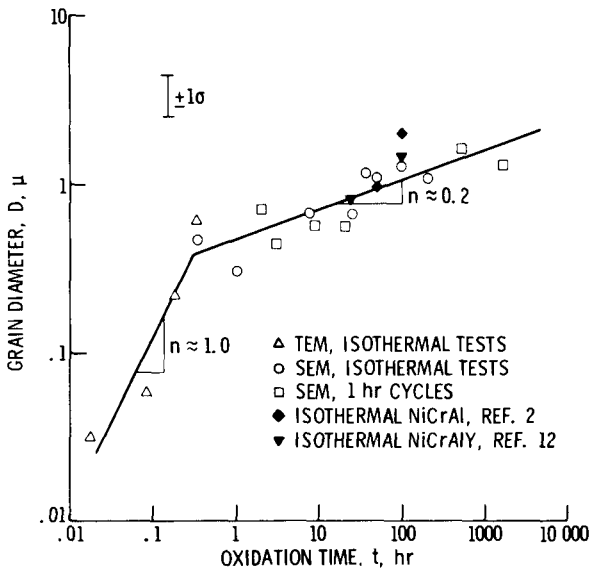

Fig. 6—Kinetics of oxide grain growth for Ni-42Al, 1100°C.

In this study the oxide lace structure in Figs. 1(*b*), 1(*c*), 3(*a*), 3(*b*), and 5(*a*) suggests preferential grain boundary diffusion of at least one species. The columnar growth at the oxide-metal interface is consistent with an inward diffusion of oxygen growth mechanism. The lack of compressive buckling of Al_2O_3 scales on NiAl is apparently associated with the columnar oxide structure, as is the case for MCrAlY alloys. It is significant that this columnar growth mechanism was inherent to the oxidation of pure NiAl, without the addition of yttrium. The similar grain sizes of the scales on NiAl, NiCrAl, and NiCrAlY (Fig. 6) suggest that grain boundary oxygen diffusion rates were also similar. This reinforces the claim that columnar Al_2O_3 grains were the result of a reduction in aluminum diffusion rates.[11] It is not clear why aluminum diffusion rates for scales on NiAl should be lower than those for scales on NiCrAl.

B. Kinetics of Oxide and Void Growth. Oxide thickness and void growth are plotted in Fig. 7. Oxide thickness was measured using SEM by inclining the specimen surface 70 deg from the horizontal plane. The fracture edge of the oxide was assumed to be perpendicular to the specimen surface in the calculation of oxide thickness. (The fractional error introduced if the oxide deviated α deg from perpendicularity is equal to tan α tan 20 deg. For estimated deviations of α = 15 deg, the thickness error was only 10 pct.) Oxide-thickness determined from metallographic cross-sections agreed with the SEM data. The cyclic and isothermal oxide thickness initially both show a linear relationship on a log x-log t plot, with time-exponents of 0.40 and 0.39, respectively. These are slightly, but measurably below the classic parabolic exponent of 0.5. (As a comparison, log-log least square fits for NiCrAl and NiCrAlY isothermal oxide thickness data taken from Ref. 2 produced a time exponent of 0.35.) After ~200 h, oxide growth for cycled specimens has become dominated by the spalling process, and the average oxide thickness has reached a maximum of ~3.5 μ. Longer isothermal tests would have accentuated the difference between isothermal and cyclic oxide thickness. However, even at 200 h, direct comparison was

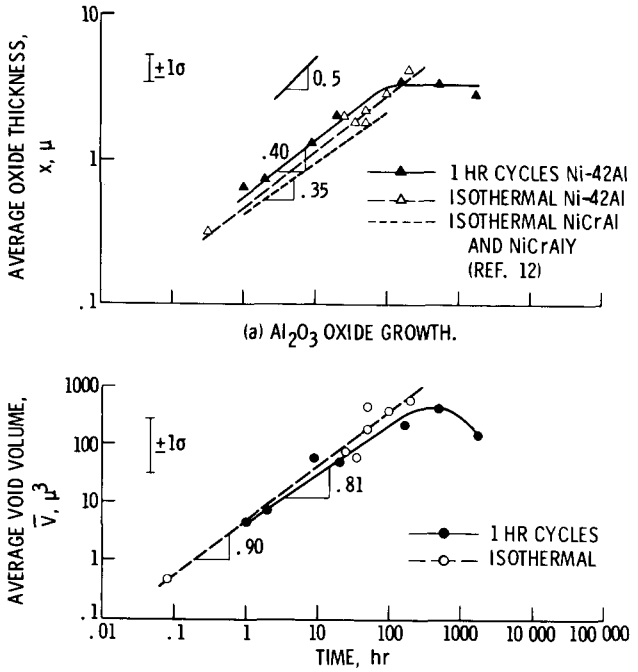

(a) Al_2O_3 OXIDE GROWTH.

(b) ESTIMATED VOID VOLUME.

Fig. 7—Oxide and void growth for Ni-42Al at 1100°C.

complicated by the formation of $NiAl_2O_4$ in the isothermal test.

The volume of individual voids was estimated by measuring their lateral dimensions and approximating them to simple geometric solids. The average void volume shown in Fig. 7(*b*) exhibited time exponents of 0.81 and 0.90 for cyclic and isothermal tests, respectively. At 500 h a maximum of ~400 μ^3 was reached for cyclic testing. The breakoff from linear behavior is similar to the oxide growth curve, occurring in the vicinity of 200 h. At this time the spalling process has exposed enough mature voids to oxidation that the average void volume was reduced.

C. Mass Balance Between Oxide and Voids. Studies of Al_2O_3 formation on MCrAl alloys[1,2,11] have discussed the formation of Kirkendall voids in the metal as a result of selective diffusion of aluminum to form the scale. Suspecting a similar phenomenon here, an attempt was made to compare the number of moles of aluminum diffused to produce the voids, M_v, with the number of moles of aluminum reacted to form the oxide, M_{ox}, where:

$$M_v = 5.6 \times 10^{-14} \text{ mole/cm}^3 \times f_v \bar{V}$$

$$M_{ox} = 7.8 \times 10^{-6} \text{ mole/cm}^3 \times \bar{x}$$

f_v void frequency, no./cm^2
$\bar{V}$ avg void vol, u^3
$\bar{x}$ avg oxide thickness, μ

M_{ox} could be calculated from $\bar{x}$ directly, while the void frequency, f_v, also had to be measured in order to calculate M_v. The results are shown in Fig. 8. The isothermal kinetics of M_v paralled those of M_{ox} quite well, with time-exponents of 0.35 and 0.39, respectively. However, the isothermal curves were significantly offset from each other such that the moles of Al/cm^2 resulting from voids were only about 1/2 of the quantity needed to grow the oxide. This implies that other mechanisms besides vacancy coalescence were also operative in accommodating excess Al vacancies. Another explanation for the discrepancy between M_{Al} and M_{ox} might be that metal recession due to oxidation has effectively reduced the void depth by removing the upper layer of the void.

The cyclic M_v curve shows a very large departure from the isothermal case, indicating that cycling (spalling) has decreased the propensity for voids to form. A plateau in cyclic M_v is expected, just as a plateau in cyclic M_{ox} has occurred, because spalling exposes the voids to oxidation. However, the excess departure of M_v at long times suggests that void formation has become a second order effect in the accommodation of Al vacancies. At 1500 h the moles of Al/cm^2 needed to form the voids was only about one-tenth of that needed to form the oxide.

The cause-effect relationship of oxides-to-voids was proven directly by a vacuum annealing experiment. A specimen run at 1150°C for 20 h at 5×10^{-5} Torr exhibited no void formation, whereas specimens oxidized under similar conditions in 1 atm air produced very evident void structures. Indeed, the void phenomenon was so strong that long time isothermal specimens had more than half the surface area occupied by voids.

Metallographic cross-sections showed no voids at distances well beneath the oxide-metal interface. This indicates that interface void formation in NiAl is not completely analogous to classical Kirkendall porosity. Oxidation-induced crystallographic voids have also been observed in pure aluminum but only at grain boundaries and at the Al_2O_3-metal interface.[13] Thus, it appears that high energy surfaces are a prerequisite for the nucleation of interface voids, while other factors, such as a high vacancy concentration, may be sufficient for the formation of internal porosity which is uniformly distributed.

II. Spalling Model

A. Model Assumptions and Curve Families. The gravimetric and oxide thickness data will be discussed in this section in relation to a mathematical model of the iterative process of oxide growth and spallation.

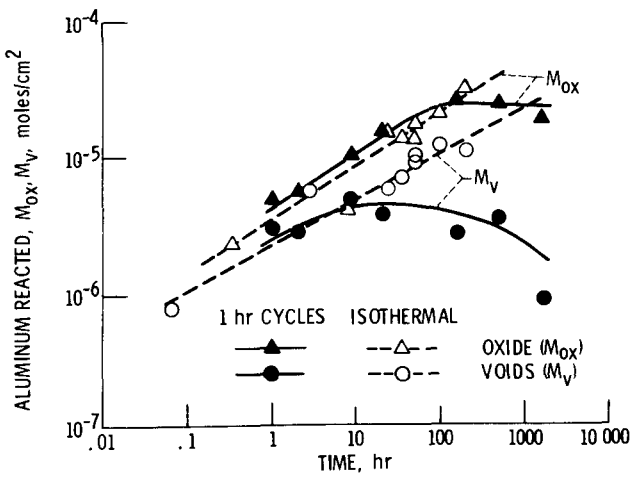

Fig. 8—Comparison of amount of aluminum reacted for oxide and void formation. (1100°C oxidation of Ni-42Al).

While the total oxide scale is initially of uniform thickness, repeated cycling will produce a composite of many oxide segments having different thicknesses.

The most general case of cyclic oxidation can be visualized as having nearly parabolic oxide growth, a random probability that a given oxide segment will spall at any given cycle, a randomly varying area spall fraction, and a randomly varying thickness spall fraction. Since this represents an infinity of possible spalling sequences, the following assumptions were made: 1) all spalling occurs at the oxide-metal interface, 2) a constant area fraction of each oxide segment, k_s, spalls off during each cooling cycle, and 3) each oxide segment grows parabolically with time.

Much basis for the first assumption can be found in the SEM studies of Section I, although limited spalling within the oxide thickness has also been observed for Ni42Al in this study. No *a priori* basis existed for the second assumption of a constant spall fraction but it does allow simplification of the mathematics. And thirdly, parabolic oxidation has been observed for Ni-50Al,[14] although data for Ni-42Al presented in Section I suggests a time-exponent closer to 0.40 rather than 0.50. The validity of these assumptions will be discussed later; at this point they appear reasonable for a first approximation of a model. A detailed description of the idealized process and a derivation of the model equations are presented in the Appendix. The resulting equations are:

$$Ox_n = \sqrt{k_p \Delta t}(1 - k_s)^n \left[\sqrt{n} + k_s \sum_{m=2}^{n} (1 - k_s)^{1-m} \sqrt{n - m + 1}\right] \quad [1]$$

$$Me_n = f_{Me} \sqrt{k_p \Delta t} \cdot k_s \sum_{i=1}^{n} \sqrt{i}(1 + (n - i)k_s)(1 - k_s)^{i-1} \quad [2]$$

$$(\Delta W/A)_n = Ox_n - Me_n \quad [3]$$

where Ox_n is the amount of oxygen weight gain in the intact oxide, and Me_n is the cumulative amount of metal lost in spalled oxide, both after n cycles. The parabolic scaling constant (k_p), the cycle time (Δt), the spall constant (k_s), and the metal-to-oxygen ratio (f_{Me}) are the inputs needed to generate model $\Delta W/A$ (specific weight change) curves.

Figures 9 and 10 show families of curves generated by the equations using f_{Me} = 1.125 for Al_2O_3. The $\Delta W/A$ curves in Fig. 9 for typical values of k_p, Δt, and k_s show that a maximum occurs followed by negative weight changes which become linear with time. The effect of increasing k_s is to decrease the number of cycles, n_o, needed to cause a negative weight change as well as increase the rate of weight loss after n_o. Increasing $k_p \Delta t$ (Fig. 9(*b*)) also causes more severe weight loss at long times, but does not change n_o or n_M, the number of cycles to reach the maximum $\Delta W/A$. The oxygen gain curves in Fig. 10 show an initial linear log-log slope of 0.50 for k_s = 0, decreasing with increasing k_s. Plateau values of the oxygen gain are also more quickly approached for larger k_s. Increasing $k_p \Delta t$ does not change the initial slope or the time at which the plateau is reached, but does increase the entire curve. And, finally, the amount of metal lost increases with both k_s and $k_p \Delta t$.

Since Eqs. [1] and [2] did not have closed form

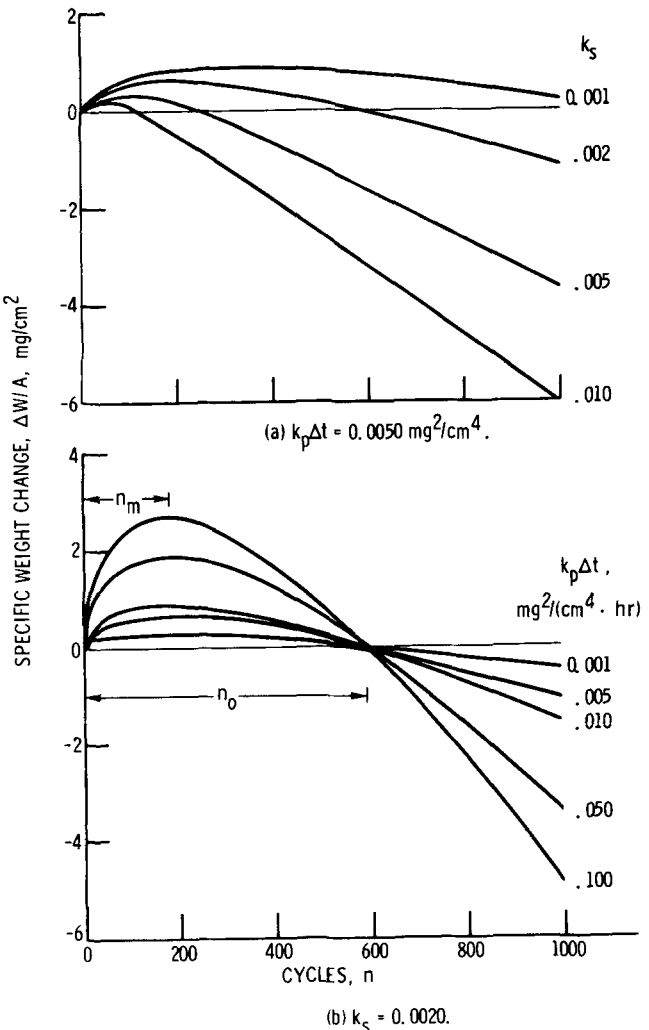

Fig. 9—Family of model curves—weight change. (*a*) $k_p \Delta t$ = 0.0050 mg²/cm⁴, (*b*) k_s = 0.0020.

solutions, $\Delta W/A$ curves had to be obtained by actual computer calculations of the summations. However, the appearance of regular features in the $\Delta W/A$ and oxygen gain curves suggested that the curves could be partially constructed by a few descriptive parameters which in turn might be simple functions of the input parameters, k_p, k_s, Δt, and f_{Me}. From series of computer runs, simple trends in some descriptive parameters were found which yielded approximate relationships with the input parameters. These relations are listed in Table I.

The descriptive parameters were simple functions of $k_p \Delta t$ for all values of k_p and Δt. Their variations with k_s were not as straightforward for large values of k_s. However, reasonable experimental values of k_s were usually ≤0.1; thus, the relations in Table I were useful here. The variations of the descriptive parameters with f_{Me} were the least well behaved and were only listed as general trends. Variations in metal loss, Me_n, did not show any characteristics amenable to descriptive parameter analysis.

B. Comparison of Oxidation Data with Model Predictions. A comparison of actual Ni-42Al, 1100°C weight-change data with some spall model curves is shown in Fig. 11. As Al_2O_3 was the primary oxide formed, f_{Me} was fixed at 1.125. Since n_o is then a

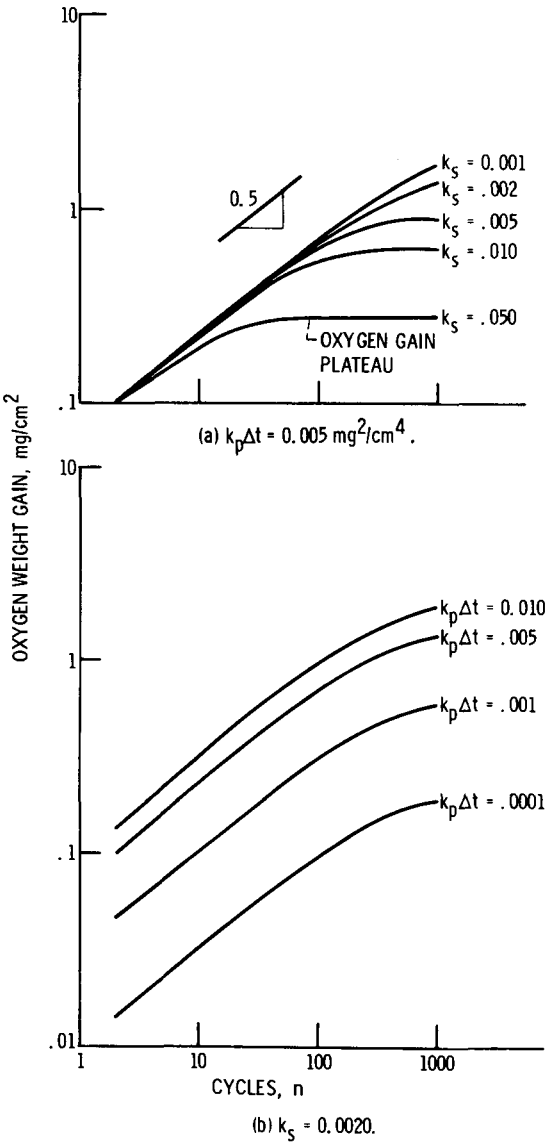

Fig. 10—Family of model curves—oxygen gained, (*a*) $k_p\Delta t$ = 0.0050 mg²/cm⁴, (*b*) k_s = 0.0020.

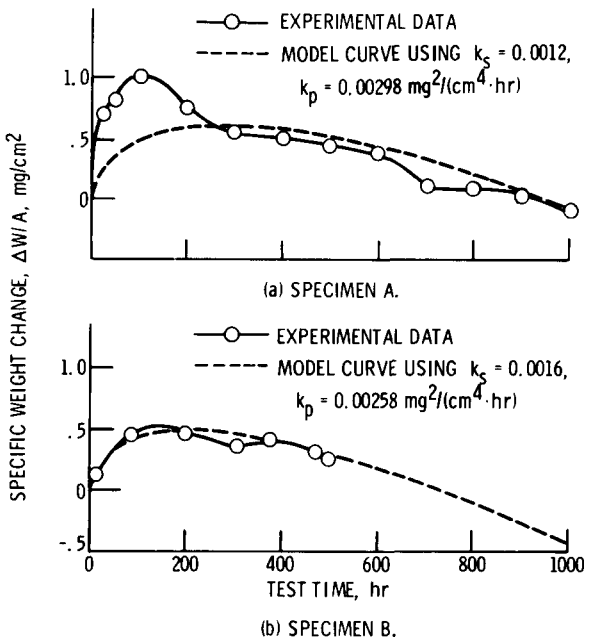

Fig. 11—Comparison of gravimetric test data with spall model curves. Ni-42Al, 1100°C, 1 h cycles. (*a*) Specimen *A*. (*b*) Specimen *B*.

function of k_s alone, k_s values could be calculated from Table I. Similarly, k_p was chosen to produce reasonable agreement with $(\Delta W/A)_{max}$. If ideal experimental curves were obtained, k_p could simply be calculated from $(\Delta W/A)_{max}$ and k_s. In the case of specimen A, however, some compromise was made between what appears to be a premature maximum and the rest of the curve. Also, if the experimental curves were ideal, n_o could be predicted from n_m and give an early indication as to how long testing must continue to produce a complete gravimetric curve. For more severe test conditions where a linear loss rate is reached, k_p can be calculated from the expression for the terminal slope. However, such conditions can often change the oxide formed, thus k_s, k_p, and f_{Me} would be altered and the model predictions would no longer apply.

Since oxide thickness is a direct measurement of oxygen gained, the thickness data from Fig. 7 was converted into mg/cm² of oxygen in Al_2O_3, using $\rho_{Al_2O_3}$ = 3.98 gm/cm³. This provided another comparison between test data and a model curve, this time for oxygen gain alone in Fig. 12. Here k_p was estimated from the plateau in oxygen gained, and k_s was estimated from the time at which the knee in the log-log curve was reached (at slope = 0.1). The model curve shown with k_s = 0.0133 fits well with the experimental data.

The agreement between calculated and experimental curves is encouraging and confirms proper trends of the model, but does not necessarily prove the assumptions made in the model. In order to provide a more critical evaluation, k_s and k_p were measured directly and independently. Parabolic plots of weight change for both iso thermal gravimetric data and for converted isothermal oxide thickness data yielded k_p = 0.0027 and 0.0030 mg²/(cm⁴ · h), respectively. The area spall fraction was measured directly by low magnification optical microscopy using polarized light. Since the Al_2O_3 oxide was optically active and the metallic surface was not, differentiation of the intact oxide from the areas where spalling to bare metal occurred was straightforward. The validity of this procedure was checked by SEM measurements, where charging effects of the nonconductive oxide allowed differentiation from the conductive bare metal areas. Average values of k_s were obtained by examining an area of ~0.25 cm² on each specimen.

The values of k_p and k_s determined by these direct measurements are compared to spall model predictions in Table II. The equation relating k_p to $(\Delta W/A)_{max}$ (Table I) predicted values of k_p very close to the measured values of k_p. However, the value calculated from the relationship of k_p to the plateau in oxygen gained was about twice the others. The actual values of k_s varied widely over the first 100 h of cyclic testing from 0.0040 to 0.1950 and did not exhibit a simple trend with time. Thus the assumption of a constant fraction of oxide spalling every cycle is incorrect. The values calculated from n_o of the weight change curves did fall within the observed range but were well below the average observed fraction of 0.041. Even the

Table I. Descriptive Parameters of Spall Model Curves

Variation with k_p, Δt, k_s ($f_{me} = 1.125$)			Variation with f_{me} ($k_s < 0.1$)	
$\Delta W/A$ versus n curve		k_s range		f_{me} range
Cycles to negative $\Delta W/A$	$n_o = 1.17\left(\frac{1-k_s}{k_s}\right) - 0.4$ cycles	0 – 0.400	$n_o \propto 1/f_{Me}$	all
Cycles to $\Delta W/A$ maximum	$n_M = 0.35\left(\frac{1-k_s}{k_s}\right) - 0.0$ cycles	0 – 0.400	$n_m \propto 1/f_{Me}$	1 - 5
Ratio n_M/n_o	$n_M/n_o = 0.30$	0 – 0.400	$n_M/n_o \cong 0.3$	1 → 10
Maximum $\Delta W/A$	$(\Delta W/A)_{MAX} = 0.39\sqrt{k_p \Delta t\left(\frac{1-k_s}{k_s}\right)}$ mg/cm^2	0 – 0.100	$\Delta W/A_{MAX} \propto \sqrt{1/f_{Me}}$	1 → 10
Terminal $\Delta W/A$ slope ($n >> n_o$)	T.S. $= -0.89\, f_{me}\sqrt{k_p \Delta t\, k_s}$ mg/cm^2/cycle	0 – 0.100	T.S. $\propto f_{Me}$	all
Oxygen weight gain versus N curve				
Terminal oxygen gain plateau	T.OX. $= 0.89\sqrt{k_p \Delta t\left(\frac{1-k_s}{k_s}\right)}$ mg/cm^2	0.001–0.100		
Cycles to oxygen plateau (when log-log slope ≈ 0.1)	$n_{0.1} = 2\left(\frac{1-k_s^2}{k_s}\right)$ cycles	0.001–0.100		

large k_s determined from $n_{0.1}$ from the oxide thickness curve was only 1/3 the measured value.

Some degree of rationalization can be made by considering the fact that the specimens were not weighed and examined every hour. Limited tests showed that weighing every cycle caused a rate of weight change of -0.44 mg/cm^2 per hundred h compared to a rate of -0.12 mg/cm^2 per hundred h when weighed over 60 h intervals. This increased spalling could be due to the additional 45°C cooling obtained upon transfer from the furnace cooling chamber to actual room conditions, longer dwell times under high humidity conditions, or simply more frequent handling of the specimens. For example, the effect of increased cooling on oxide spalling of Ni-base alloys was found to be significant.[15] The difference in weight loss corresponding to cooling to 65°C compared to cooling to 20°C was on the order of 0.25 mg/cm^2 after 195 one hour cycles at 1100°C. Also, tensile testing Al_2O_3 filaments[16] has shown that slow crack growth occurs in a water environment as a stress corrosion phenomenon. Indeed, a 5-day isothermal exposure of the oxidized Ni-42Al specimens to 80°C saturated air caused oxide spalling of 0.12 mg/cm^2. Whether humidity, excess cooling, or other factors were respondible, the values of k_s measured optically are likely to be higher than the actual ones, unless extended cooling to room temperature would be used each test cycle.

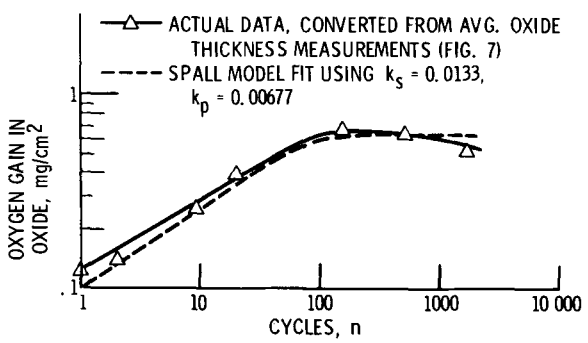

Fig. 12—Comparison of oxygen pickup with spall model curve. Ni-42Al, 1100°C, 1 h cycles.

The difference in the values of k_s calculated from the gravimetric curve (from n_o) with that calculated from the oxide thickness curve (from $n_{0.1}$) is more difficult to explain. The experimental error in the gravimetric curve was insignificant, so that little error in the calculated value of k_s could be rationalized. There was more scatter in the oxide thickness curve, but not enough to change k_s by an order of magnitude. To effect this, $n_{0.1}$ would have to be increased from its 150 h to 1500 h, which is clearly unreasonable from Fig. 12. It is also difficult to postulate how the oxide thickness could prematurely level off without simultaneously causing the gravimetric curve to decrease more rapidly than it did.

C. Dependence of k_s on Oxide Thickness. Returning to the observation that k_s varies with time, some important differences between isothermal and cyclic k_s values are shown in Fig. 13. (Isothermal k_s is the

Table II. Comparison of Measured k_p and k_s with Values Calculated From Spall Model Relations (Ni-42Al, 1100°C, f_{Me} = 1.125)

Method of determination	k_p, mg^2/cm^4 · h	k_s
(A) Direct measurement		
Thermobalance isothermal gravimetric curve	0.0027	
Converted isothermal oxide thickness	.0030	
Polarized light micrographs, 1-hour cycles, fig. 13 (between 1 and 1500 hours)		0.0040–0.1950 (0.041 avg)
(B) Inferred from spall model (1-hour cycles)		
Gravimetric curve, Fig. 11(a)	0.0030	0.0012
Gravimetric curve, Fig. 11(b)	.0026	.0016
Oxide thickness curve, Fig. 12	.0068	.0133

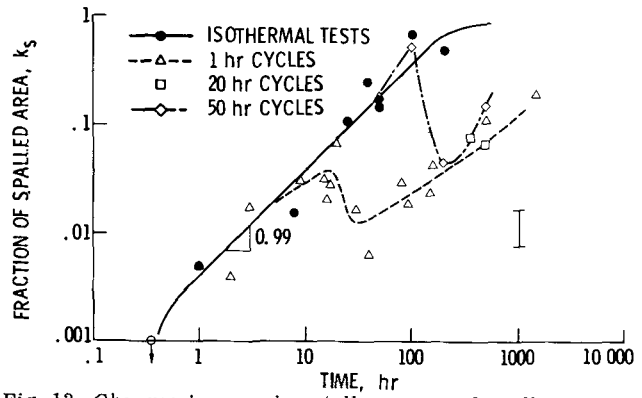

Fig. 13—Changes in experimentally measured spall parameter with oxidation time for Ni-42Al at 1100°C.

spalled area fraction measured after one cycle.) As mentioned previously, the one-hour cycle tests showed considerable scatter in k_s. Definite upward trends did not exist for the entire curve. However, the isothermal k_s increased continually with a time-exponent 1.0, even reaching $k_s = 0.70$ for a 100-h test. According to the model the terminal weight loss rate varies as $\sqrt{k_p k_s/\Delta t}$ mg/(cm^2 · h) (Table I). Thus, if $k_s/\Delta t$ increases, the severity of the test also increases. In order to check if $k_s/\Delta t$ could increase with Δt, tests were run using 20 and 50 h cycles. The weight change data for these long cycle tests is compared to the one-hour data in Fig. 14. A considerable increase in spalling has occurred just by lengthening the test cycle. On the basis of the spall model, both the 20 and 50 h cycle data predict $k_s = 0.1225$, nearly two orders of magnitude greater than the 1 h cycle value of 0.0016. For an equal amount of test time the 20 h cycle test was the most severe.

The variation of k_s with cycle frequency and oxidation time complicates the analysis in terms of a simplified phenomenological spall model. A complete theoretical model should be able to predict variations in k_s *a priori*, such as by consideration of mechanical properties and stress distributions in the oxide. Figure 15 shows that k_s for isothermal tests varied as (oxide thickness),[2] suggesting that thicker oxides were more highly stressed. The cyclic k_s data exhibited a considerable degree of scatter, but seemed to follow the isothermal data more closely here than when plotted as a function of time (Fig. 13). The implication is that k_s is a strong function of oxide thickness for the first few cycles, which degenerates somewhat with continued cycling. Thus the stress model for spalling of a continuous oxide sheet should predict a high degree of thickness dependence, whereas the model for spalling of a topographically complex oxide composed of many segments should be less thickness dependent.

A discussion of oxide stress models does show an oxide interfacial shear stress dependence on x/L, where L is the length of an oxide plate.[17] The observed increase in k_s with oxide thickness would support such a model. However, the observation that the large intact oxide plates (large L) in isothermal tests spalled more than the small segments of the same thickness in cyclic tests (Fig. 15) does not agree with such a stress model. Perhaps the severe void condition for the isothermal tests requires a consideration

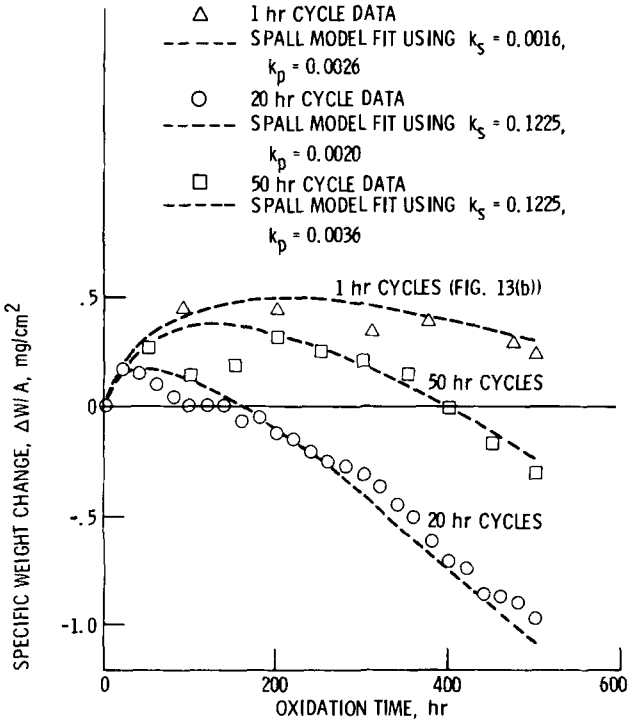

Fig. 14—Effect of cycle frequency on oxidation of Ni-42Al at 1100°C.

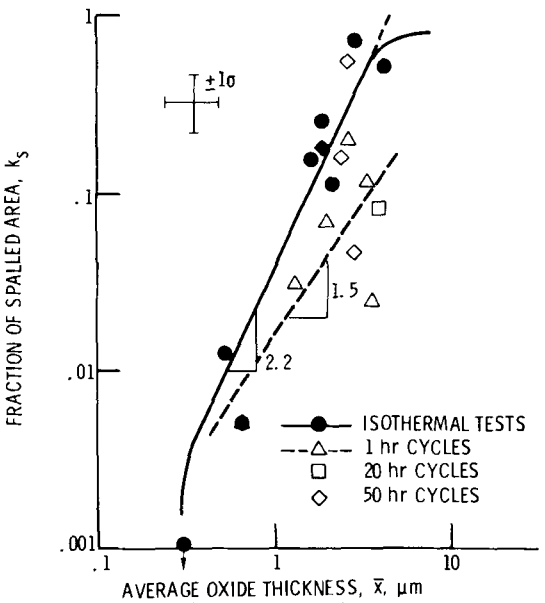

Fig. 15—Dependence of experimentally measured spall parameter on oxide thickness for Ni-42 at. pct Al, 1100°C.

of bending stress as well as shear stress to successfully predict trends in k_s.

SUMMARY OF RESULTS

Ni-42 at. pct Al specimens were oxidized at 1100°C in cyclic and isothermal tests. The morphology of the Al_2O_3 scale and metal surface was studied by SEM. An attempt to describe the cyclic oxidation behavior by a parabolic growth and constant spall fraction model was made. The following results were obtained:

1) Oxide spalling occurred primarily at the oxide-metal interface in an intergranular mode.

2) Crystallographic Kirkendall voids occurred as a result of oxidation. The total void volume kinetics followed those of oxide growth for isothermal tests, but fell increasingly behind for long-term cyclic tests.

3) A spall model was developed in the form of a summation series. While no closed form of the series was found, good approximations of critical points on the gravimetric curve could be made as a function of k_p and k_s. Model curves were found to fit monotonic gravimetric curves reasonably well. However, experimentally determined values of k_s were typically higher than those obtained from fitting model curves to the data.

4) The fractional area of spalled oxide varied widely in cyclic tests but increased with (oxide thickness)^2 for isothermal tests.

CONCLUDING REMARKS

The interfacial spalling mode of Ni-42Al was typical for alloys having no rare-earth additions where the oxide-metal bond is weak relative to the oxide itself. However, the 1100°C oxidation resistance of Ni-42Al coupons was reasonably good in 1 h cycle tests. On the other hand MCrAl alloys without oxygen-active metal additions show more rapid deterioration in cyclic cyclic oxidation (1 mg/cm^2 loss in 20 h at 1100°C).[2] Because these MCrAl alloys have a lower level of aluminum (*e.g.*, 12 at. pct), Al_2O_3 formation and spalling might cause sufficient depletion at the surface to allow spinel and monoxides to form. The dramatic improvements caused by yttrium additions may not occur for alloys where the aluminum level is high enough to sustain Al_2O_3 formation after repeated spalling. The role of oxide pegging caused by rare earth additions, which was precluded by the use of pure Ni-42Al, would also be diminished for high aluminum alloys. The void problem seemed to be self-healing by repeated cycling so that the creation of vacancy sinks due to yttrium additions would also appear to be unnecessary for void elimination. The columnar growth of the scale at the oxide-metal interface was consistent with an oxygen grain boundary diffusion oxidation mechanism. It is noteworthy that this columnar Al_2O_3 growth has previously been associated only with adherent scales formed on MCrAlY alloys.

The use of any mathematical spall model to fit cyclic oxidation behavior must be approached with caution. Other models (continuous oxide spalling or a step-process constant fractional thickness spall) will also fit the data with reasonable values of k_p and k_s. A good data fit may be useful for predictions but does not necessarily indicate the detailed spalling mechanisms. The attempt in this work to correlate model values with experimentally observed values of the spalled area fraction was frought with difficulties. Perhaps the most important outcome is pointing out that the experimental determinations of k_s will require a very closely controlled procedure in which the measurement is an integral part of the actual oxidation test. The stochastic process, where k_s is allowed to vary randomly from one oxide segment to another, was not treated. However, the observed trends in direct measurements of spalled area fractions do suggest that thicker oxide plates have larger k_s values. While no perfect relationship was observed, any restrictions placed on a truly random spall probability will be of use in simplifying future models.

In view of the oxide thickness dependence of k_s here, the formulation and testing of stress models to predict such a relationship could prove to be a fruitful area of study. Any insight into the failure mechanisms (interfacial shear, bending) would be significant. However, the ultimate task of incorporating such mechanisms into a model which presumes a transition from a uniform oxide sheet to segments of various areas and thicknesses will not be trivial.

APPENDIX

The basic assumptions of the spalling model developed here are 1) growth of each oxide segment occurs parabolically for the duration of the heating cycle, and 2) a constant fraction of all oxide segments present spalls off at the oxide-metal interface after each cooling cycle. The competing processes of oxide growth and spallation are illustrated schematically for the first three cycles in Fig. 16. In this figure the fraction spalled per cycle is 1/2 for the sake of clarity. O_{mn} and S_{mj} refer to the specific oxide segments and their spalled counterparts and are the "building blocks" for the derivation of the iteration equation. It should be pointed out that from a mathematical standpoint it is equivalent to have spalling occur at multiple locations within a given segment of specific thickness. Figure 16 shows all the spalling occurring at one location for the sake of clarity.

Following is a list of definitions used in the derivation:

- m cycle number at which oxide segment started growth,
- j cycle number at which oxide segment spalled off,
- n total number of cycles passed,

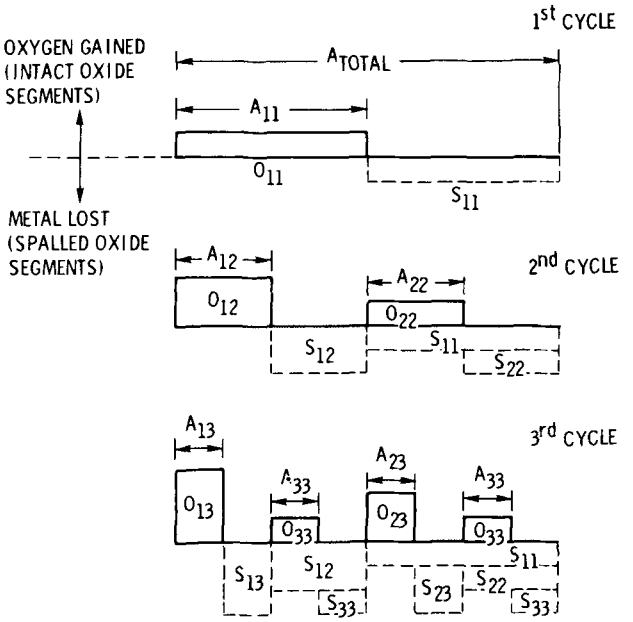

Fig. 16—Schematic of spalling model.

O_{mn} oxygen weight gain of intact segment m, n (mg/cm^2),
A_{mn} fractional area of intact segment m,n,
X_{mn} "thickness" of intact segment m, n (mg/cm^2),
Ox_n total oxygen weight of intact segments after n cycles (mg/cm^2),
S_{mj} weight of metal in spalled oxide segment m, j (mg/cm^2),
A_{mj} fractional area of spalled segment m, j
X_{mj} "thickness" of spalled segment m, j (mg/cm^2),
f_{Me} ratio of metal-to-oxygen in oxide (1.125 for Al_2O_3),
Me_n total weight of metal lost after n cycles (mg/cm^2),
$\Delta W/A$ specific weight change (mg/cm^2),
k_p parabolic oxidation constant (mg^2/(cm^4 · h)),
k_s spall fraction constant, and
Δt heating cycle time (h).

Summing all the oxygen gains in segments which have not spalled gives the total oxygen gained at n cycles:

$$Ox_n = \sum_{m=1}^{n} O_{mn} \qquad [A1]$$

where $O_{mn} = X_{mn}A_{mn}$. For metal loss, the spalled weight for the n-th cycle ($j = n$) must be summed, $\sum_{m=1}^{j} S_{mj}$, as well as for all previous cycles ($j < n$), in order to yield the total spalled weight:

$$Me_n = \sum_{j=1}^{n} \sum_{m=1}^{j} S_{mj} \qquad [A2]$$

where

$$S_{mj} = f_{Me} \cdot X_{mj}A_{mj}. \qquad [A3]$$

Finally,

$$(\Delta W/A)_n = Ox_n - Me_n. \qquad [A4]$$

From Fig. 16, the progression of oxide segment areas m, n follows a power law, where $(1 - k_s)$ is representative of the unspalled segment area, while k_s represents the spalled fraction.

The fractional area of the m, n-th segment is given by

$$\left.\begin{aligned} A_{1n} &= (1 - k_s)^n;\ m = 1 \\ A_{mn} &= (1 - k_s)^{n-(m-1)} k_s;\ m \geq 2. \end{aligned}\right\} \qquad [A5]$$

The thicknesses grow parabolically with the residence time of Δt times the number of growth cycles:

$$X_{mn} = \sqrt{k_p \Delta t} \cdot \sqrt{n - m + 1}. \qquad [A6]$$

From a knowledge of A_{mn} and X_{mn}, Ox_n can be calculated from Eq. [A1]:

$$Ox_n = \sqrt{k_p \Delta t}(1 - k_s)^n\left[\sqrt{n} + k_s \sum_{m=2}^{n} (1-k_s)^{1-m}\sqrt{n-m+1}\right]. \qquad [A7]$$

The amount of aluminum spalled for a spalled segment m, j is given by:

$$\left.\begin{aligned} S_{1j} &= f_{Me}\sqrt{k_p \Delta t} \cdot \sqrt{j}\, k_s(1 - k_s)^{j-1};\ m = 1 \\ S_{mj} &= f_{Me}\sqrt{k_p \Delta t} \cdot \sqrt{j - m + 1}\, k_s^2(1 - k_s)^{j-m};\ m \geq 2. \end{aligned}\right\} \qquad [A8]$$

By summing $\sum_{j=1}^{n} \sum_{m=1}^{j} S_{mj}$ for the first four cycles, a single summation series becomes evident from the double sum, and the amount of aluminum spalled is given by:

$$Me_n = f_{Me} \cdot \sqrt{k_p \Delta t} \cdot k_s \sum_{i=1}^{n} \sqrt{i}\,(1 + (n - i)k_s) \times (1 - k_s)^{i-1}. \qquad [A9]$$

While it is concise to represent Ox_n and Me_n by convolution-summation series, no closed form solution was found to exist. Attempts at an approximate solution by integration were also unsuccessful. An abbreviated form of the Ox_n series was found, which simplified hand calculation somewhat:

$$Ox_n = \sqrt{k_p \Delta t} \sum_{m=1}^{n} \frac{(1 - k_s)^m}{\sqrt{m} + \sqrt{m-1}} \text{ (convergent for } k_s < 1). \qquad [A10]$$

Since the series is convergent as $n \to \infty$, there is an asymptotic value of Ox_n which is referred to in the report as terminal oxygen gain.

REFERENCES

1. J. K. Tien and F. S. Pettit: *Met. Trans.*, 1972, vol. 3, p. 1587.
2. C. S. Giggins and F. S. Pettit: PWA Report 5364, Pratt & Whitney Aircraft, East Hartford, Conn., June 1975.
3. C. A. Barrett and C. E. Lowell: NASA TN D-8255, June 1976.
4. J. L. Smialek and C. E. Lowell: *J. Electrochem. Soc.*, 1974, vol. 121, p. 800.
5. C. A. Barrett and A. F. Pressler: NASA TN D-8132, February 1976.
6. C. E. Lowell: unpublished research, NASA Lewis Research Center, Cleveland, Ohio, 1975.
7. S. R. Levine: unpublished research, NASA Lewis Research Center, Cleveland, Ohio, 1972.
8. J. L. Smialek and R. F. Hehemann: *Met. Trans.*, 1973, vol. 4, p. 1571.
9. C. M. Kapadia and M. H. Leopold: *The Mechanism of Grain Growth in Ceramics*, University of Kentucky, Lexington, Kentucky.
10. R. L. Coble: *J. Appl. Phys.*, 1961, vol. 32, p. 793.
11. F. A. Golightly, F. H. Stott, and G. C. Wood: *Oxidation of Metals*, 1976, vol. 10, p. 163.
12. C. S. Giggins and F. S. Pettit: PWA Report 4786, Pratt and Whitney Aircraft, Hartford, Conn., July 1973.
13. C. Roques-Carmes, *et al.*: *Metallography*, 1971, vol. 4, p. 385.
14. G. J. Santoro, D. L. Deadmore, and C. E. Lowell: NASA TN D-6414, July 1971.
15. D. Deadmore and C. Lowell: *Oxidation of Metals*, 1977, vol. 11, p. 91.
16. D. M. Kotchick and R. E. Tressler: *J. Mater. Sci.*, 1975, vol. 10, p. 608.
17. J. K. Tien and J. M. Davidson: *Stress Effects and the Oxidation of Metals*, J. V. Cathcart, ed., pp. 200-19, Am. Inst. Min., Metall. Pet. Eng., Inc., New York, 1975.